Monthly Notices
of the
ROYAL ASTRONOMICAL SOCIETY

MNRAS **493,** 3920–3931 (2020)
Advance Access publication 2020 February 13

doi:10.1093/mnras/staa443

Effective spin distribution of black hole mergers in triples

Giacomo Fragione [1,2]★ and Bence Kocsis[3]

[1]*Department of Physics & Astronomy, Northwestern University, Evanston, IL 60202, USA*
[2]*Center for Interdisciplinary Exploration & Research in Astrophysics (CIERA), Evanston, IL 60202, USA*
[3]*Institute of Physics, Eötvös University, Pázmány P. s. 1/A, Budapest 1117, Hungary*

Accepted 2020 February 11. Received 2020 February 11; in original form 2019 September 26

ABSTRACT

Many astrophysical scenarios have been proposed to explain the several black hole (BH) and neutron star binary mergers observed via gravitational waves (GWs) by the LIGO–Virgo collaboration. Contributions from various channels can be statistically disentangled by mass, spin, eccentricity, and redshift distributions of merging binaries. In this paper, we investigate the signatures of BH–BH binary mergers induced by a third companion through the Lidov–Kozai mechanism in triple systems. We adopt different prescriptions for the supernovae natal kicks and consider different progenitor metallicities and initial orbital parameters. We show that the typical eccentricity in the LIGO band is 0.01–0.1 and that the merger rate is in the range $0.008-9\,\mathrm{Gpc^{-3}\,yr^{-1}}$, depending on the natal kick prescriptions and progenitor metallicity. Furthermore, we find that the typical distribution of effective projected spin is peaked at $\chi_{\rm eff} \sim 0$ with significant tails. We show that the triple scenario could reproduce the distribution of $\chi_{\rm eff}$. We find that the triple channel may be strongly constrained by the misalignment angle between the binary component spins in future detections with spin precession.

Key words: black hole physics – stars: kinematics and dynamics – stars: neutron – Galaxy: kinematics and dynamics – galaxies: kinematics and dynamics.

1 INTRODUCTION

Many astrophysical scenarios have been proposed to explain the several black hole (BH) and neutron star (NS) binary mergers observed via gravitational wave (GW) emission by the LIGO–Virgo collaboration. Possibilities include isolated binary evolution (Belczynski et al. 2016; Kruckow et al. 2018), mergers catalyzed by stellar envelope expansion (Tagawa, Saitoh & Kocsis 2018), mergers in star clusters (Askar et al. 2017; Banerjee 2018; Fragione & Kocsis 2018; Rodriguez et al. 2018), mergers in galactic nuclei (O'Leary, Kocsis & Loeb 2009; Antonini & Perets 2012; Grishin, Perets & Fragione 2018; Fragione et al. 2019a; Hamilton & Rafikov 2019; Rasskazov & Kocsis 2019), mergers in gaseous discs (Bartos et al. 2017; Stone, Metzger & Haiman 2017; Tagawa, Haiman & Kocsis 2019), and Lidov–Kozai (LK) mergers in isolated triple and quadruple systems (Antonini, Toonen & Hamers 2017; Silsbee & Tremaine 2017; Arca-Sedda, Li & Kocsis 2018; Fragione & Kocsis 2019; Liu & Lai 2019).

With the improving sensitivity of LIGO–Virgo and the expected commissioning of KAGRA and LIGO India, hundreds of detections of merging systems are expected within the decade. Thus, it is fundamental to provide tools to distinguish among the mergers that originate in different astrophysical channels. It has been shown that useful parameters that can help doing so are the masses, spins, eccentricity, and redshift of the merging binaries. Their distributions can be used as an indicator to statistically disentangle among the contributions of the several scenarios. This includes identifying correlations between mass and eccentricity (Breivik et al. 2016; Gondán et al. 2018), mass and spins (Postnov & Kuranov 2017; Arca Sedda & Benacquista ; Yang et al. 2019a), the mass distribution (Stevenson, Ohme & Fairhurst 2015; O'Leary, Meiron & Kocsis 2016; Fishbach, Holz & Farr 2017; Mandel et al. 2017; Zevin et al. 2017; Kocsis et al. 2018; Perna et al. 2019; Yang et al. 2019b), the spin distribution (Fishbach et al. 2017), eccentricity distribution in the LIGO/Virgo band (Wen 2003; O'Leary et al. 2009; Cholis et al. 2016; Arca-Sedda et al. 2018; Gondán et al. 2018; Samsing et al. 2018; Zevin et al. 2019) and in the LISA band (O'Leary et al. 2006; Nishizawa et al. 2016, 2017; D'Orazio & Samsing 2018; Samsing & D'Orazio 2018), spin orientations (Rodriguez et al. 2016; Liu & Lai 2017, 2018; Stevenson, Berry & Mandel 2017; Talbot & Thrane 2017; Vitale et al. 2017a; Farr, Holz & Farr 2018; Gerosa et al. 2018; Liu & Lai 2018; Lopez et al. 2019), the projected effective spin parameter (Antonini et al. 2018; Ng et al. 2018; Schrøder, Batta & Ramirez-Ruiz 2018; Zaldarriaga, Kushnir & Kollmeier 2018), and other waveform features (Inayoshi et al. 2017; Meiron, Kocsis & Loeb 2017; Kremer et al. 2018; Samsing et al. 2018, 2019).

GW emission is highly efficient at circularizing the orbit of an inspiraling binary. As a consequence, BHs that merge in isolation

★ E-mail: giacomo.fragione@northwestern.edu

are expected to enter the LIGO frequency band (10 Hz) almost circular, with typical eccentricities in the range $e_{10\rm Hz} \sim 10^{-7}$–$10^{-6}$. In the case the BH binary merges in a hierarchical system as a result of the LK mechanism, a number of authors showed that the typical eccentricity has much higher values, in the range $\sim 10^{-2}$–10^{-1} (Wen 2003; Antonini et al. 2016; Fragione & Bromberg 2019; Fragione & Kocsis 2019; Fragione & Loeb 2019). If the BH binary is dynamically assembled in a cluster environment, the spectrum of possible eccentricities is rich, with three possible outcomes (Samsing & D'Orazio 2018; Zevin et al. 2019): (i) binaries that are ejected and merge outside the cluster have eccentricities $\sim 10^{-7}$–10^{-6}, as in the isolated binary case; (ii) binaries that merge as a result of a GW capture process have eccentricities $\sim 10^{-2}$–10^{-1}, as in the LK-induced mergers; (iii) binaries that merge within the cluster have intermediate eccentricities $\sim 10^{-5}$–10^{-3}. The recent non-detection of eccentric sources by LIGO–Virgo was used to place an upper limit on the rate of eccentric mergers with $e_{10\rm Hz} > 0.1$ of $\mathcal{R} \leq 300\, f_{\rm ecc}\, {\rm Gpc^{-3}yr^{-1}}$, where $f_{\rm ecc}$ is the fraction of mergers with $e_{10\rm Hz} > 0.1$ (LIGO Scientific Collaboration 2019b). In comparison, the rate density of circular mergers is between 28 and 104 $\rm Gpc^{-3}\, yr^{-1}$ for a power-law mass distribution prior (LIGO Scientific Collaboration 2019a). The eccentricity of dynamically formed BH binaries is much higher in the GW frequency band of LISA.

Another powerful quantity to discriminate among the contributions of different astrophysical merger channels is $\chi_{\rm eff}$, the effective spin of the BH binary at merger defined as the mass-weighted average of the binary components' spins projected on to the orbital angular momentum vector of the binary. Binaries that evolve and merge in isolation are expected to have spin vectors that are aligned with the orbital angular momentum vector of the binary mainly due to tidal dissipation effects (Vitale et al. 2017a; Gerosa et al. 2018). BHs that merge in star clusters are instead expected to have spin vectors distributed isotropically, as a consequence of the fact that the dynamical binary assembly does not prefer any specific direction (Rodriguez et al. 2016; Arca Sedda & Benacquista 2019). For what concerns the focus of this work, LK-induced mergers in triple systems, Antonini et al. (2018) and Rodriguez & Antonini (2018) claimed that the BH binary component spins typically align in the perpendicular direction with respect to the orbital angular momentum of the binary due to the tertiary companion in a triple system, implying near-zero effective spins at merger. However, even more recently, Liu, Lai & Wang (2019) have shown that these findings are sensitive to the applied approximations and orbit averaging in the equations of motion. They showed that the BH spin exhibits a wide range of evolutionary paths, and different distributions of final spin–orbit misalignments can be produced depending on the system parameters.

In this paper, we study the dynamical evolution of BH triples by means of high-precision direct *N*-body simulations, including post-Newtonian (PN) terms up to 2.5PN order. We start from the main-sequence progenitors of the BHs and model the supernova (SN) events that lead to the formation of the BH triple. We adopt different prescriptions for the SN natal kicks, and consider different progenitor metallicities and orbital parameters. We determine the expected distributions of various properties of merging systems, including masses, eccentricities, spin–orbit misalignment, and merger times.

The paper is organized as follows. In Section 2, we discuss the initial conditions adopted in this paper. In Section 3, we discuss the distribution of masses, orbital parameters, eccentricities, and spin–orbit misalignments of merging systems. Finally, in Section 4, we discuss the implications of our findings and draw our conclusions.

2 INITIAL CONDITIONS

The stellar triples in our simulations are initialized as described in what follows. In total, we consider nine different models (see Table 2).

We consider a triple system comprised of an inner binary of mass $m_{\rm in} = m_1 + m_2$ and a third body of mass m_3 that orbits the inner binary. The semimajor axis and eccentricity of the inner orbit are $a_{\rm in}$ and $e_{\rm in}$, respectively, and the semimajor axis and eccentricity of the outer orbit are $a_{\rm out}$ and $e_{\rm out}$, respectively. The inner and outer orbital plane have initial relative inclination i_0.

We sample the mass m_1 of the most massive star in the inner binary from an initial mass function

$$\frac{{\rm d}N}{{\rm d}m} \propto m^{-\beta}, \tag{1}$$

in the mass range 20–150 $\rm M_\odot$, reflecting the progenitor of the BH. We fix $\beta = 2.3$ (Kroupa 2001). We adopt a flat mass ratio distribution for the inner binary, m_2/m_1, and the outer binary, $m_3/(m_1 + m_2)$ (Sana et al. 2012; Duchêne & Kraus 2013; Sana 2017). The mass of the secondary in the inner binary and of the third companion are sampled from the range 20–150 $\rm M_\odot$. For comparison, we also estimate how the final rate changes if the mass ratio distribution is assumed to be loguniform (Sana et al. 2013).[1]

We take the distribution of the inner and outer semimajor axis, $a_{\rm in}$ and $a_{\rm out}$, respectively, loguniform (Kobulnicky et al. 2014). In order to make sure that the periapsis distance of the inner binary is large enough that no common envelope phase or mass transfer occurs,[2] we set a minimum orbital separation $a_{\rm in}(1 - e_{\rm in}^2) \gtrsim 10$ au (Antonini et al. 2017). We adopt three values for the maximum separation of the triple respectively in different simulation sets, $a_{3,\rm max} = 2000$, 3000, and 5000 au, see Table 2 (Sana et al. 2014). For the orbital eccentricities of the inner binary, $e_{\rm in}$, and outer binary, $e_{\rm out}$, we assume a flat distribution. The initial mutual inclination i_0 between the inner and outer orbit is drawn from an isotropic distribution, while the other relevant angles (i.e. argument of periapsis, argument of node, mean anomaly) are drawn randomly.

After sampling the relevant parameters, we check that the initial configuration satisfies the stability criterion of hierarchical triples of Mardling & Aarseth (2001).

Given this set of initial conditions for the stellar triples, we assume that each of the three stars in the triple undergoes an SN event sequentially. We assume that SNe take place instantaneously (on a time-scale shorter than the orbital period), during which a given star loses mass instantaneously and collapses to a BH (for details see e.g. Pijloo, Caputo & Portegies Zwart 2012; Toonen, Hamers & Portegies Zwart 2016; Fragione & Loeb 2019).[3] We determine the final masses of the BHs by using the fitting formulae to the results of the PARSEC stellar evolution code (see appendix C in Spera, Mapelli & Bressan 2015). We adopt five different values of the progenitor metallicity as shown in Table 2, $Z = 0.0001$, 0.001,

[1] From observations, Duchêne & Kraus (2013) found that $f(q) \propto q^{1.16 \pm 0.16}$ and $q^{-0.01 \pm 0.03}$ for solar type stars with period less than or larger than $10^{5.5}$ d, respectively, while Sana et al. (2013) found $f(q) \propto q^{-1.0 \pm 0.4}$ for massive O-type stars.

[2] This would also shrink the inner orbit and make the LK mechanism strongly suppressed by the relativistic precession (see e.g. Naoz 2016).

[3] We ignore the SN-shell impact on the companion stars.

0.005, 0.01, and 0.015, which ultimately sets the final mass of the BH remnant.

As a result of the mass-loss, the exploding star is imparted a kick to its centre of mass (Blaauw 1961), and the system receives a natal kick due to recoil from an asymmetric SN explosion. We assume that the BH natal velocity kick is drawn from a Maxwellian distribution

$$p(v_{\rm k}) \propto v_{\rm k}^2 {\rm e}^{-v_{\rm k}^2/\sigma^2}, \quad (2)$$

with a velocity dispersion σ. In our fiducial model, we consider $\sigma = 260\,{\rm km\,s^{-1}}$ for NSs, consistent with the distribution deduced by Hobbs et al. (2005). We run an additional model where we set $\sigma = 100\,{\rm km\,s^{-1}}$, consistent with the distribution of natal kicks found by Arzoumanian, Chernoff & Cordes (2002). We also adopt a model where no natal kick is imparted during BH formation (see Table 2). For BHs, we implement momentum-conserving kicks, in which we assume that the momentum imparted to a BH is the same as the momentum given to an NS (Fryer & Kalogera 2001). As a consequence, the kick velocities for the BHs is lowered by a factor of $1.4\,{\rm M}_\odot/m_{\rm BH}$ with respect to NSs. The value of σ is highly uncertain.

After each SN event, the orbital elements of the triple are updated as appropriate (see e.g. Fragione et al. 2019c), to account both for mass-loss and natal kicks. The final masses of the BHs in the inner binary are $m_{\rm BH,1}$ and $m_{\rm BH,2}$, and the outer companion $m_{\rm BH,3}$. We also check that the stability criterion of hierarchical triples of Mardling & Aarseth (2001) is satisfied and the triple is stable following mass-loss and natal kicks. After all the SNe took place, we integrate the triple systems by means of the ARCHAIN code (Mikkola & Merritt 2006, 2008), including PN corrections up to order 2.5PN. We perform ∼750–1000 simulations for each model in Table 2. We fix the maximum integration time as (Silsbee & Tremaine 2017),

$$T = \min(10^3 \times T_{\rm LK}, 10\ {\rm Gyr}), \quad (3)$$

where $T_{\rm LK}$ is the triple LK time-scale (Antognini 2015)

$$T_{\rm LK} = \frac{8}{15\pi}\frac{m_{\rm tot}}{m_{\rm BH,3}}\frac{P_{\rm out}^2}{P_{\rm in}}\left(1-e_{\rm out}^2\right)^{3/2}, \quad (4)$$

where $m_{\rm tot} = m_{\rm BH,1} + m_{\rm BH,2} + m_{\rm BH,3}$ and $P_{\rm in}$ and $P_{\rm out}$ are the inner and outer orbital period, respectively.

3 RESULTS

In our simulations, we find that ∼5 per cent–8 per cent of the triple systems lead to a merger of the inner binary. In the following subsections, we investigate the distribution of these mergers with respect to masses, orbital parameters, and spins.

3.1 Mass distribution

Fig. 1 shows the cumulative distribution function (CDF) of the total BH mass of BH–BH binaries in triples that lead to a merger, for different values of Z (top panel; $\sigma = 260\,{\rm km\,s^{-1}}$) and σ (bottom panel; $Z = 0.01$). Both Z and σ affect the distribution of total BH masses.

For $Z \lesssim 0.005$, the distributions do not depend significantly on the progenitor metallicity and the total BH mass is limited to $\sim 60\,{\rm M}_\odot$. For higher metallicities, the progenitors can collapse to more massive BHs, up to $\sim 120\,{\rm M}_\odot$–$140\,{\rm M}_\odot$ (Spera et al. 2015). We find that ∼50 per cent of the mergers have total mass $\gtrsim 90\,{\rm M}_\odot$ and $\gtrsim 120\,{\rm M}_\odot$ for $Z = 0.001$ and $Z = 0.0001$, respectively. This

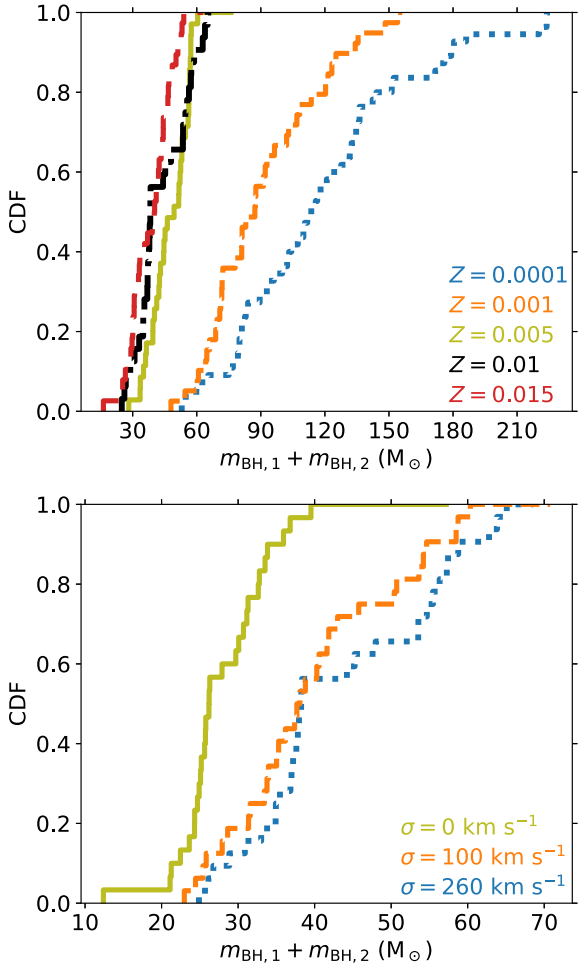

Figure 1. Cumulative distribution function of the total BH mass of BH–BH binaries in triples that lead to a merger, for different values of progenitor metallicity Z (top; $\sigma = 260\,{\rm km\,s^{-1}}$) and σ (bottom; $Z = 0.01$).

is consistent with the findings of Fragione & Loeb (2020). For comparison, we report the distribution of total masses inferred from LIGO–Virgo mergers and the IAS group (LIGO Scientific Collaboration 2019a; Venumadhav et al. 2019; Zackay et al. 2019) in Table 1. We note that population of very massive binaries we find in our simulations may be due to the fact that we are using fitting formulae to single stellar evolutionary tracks to determine the BH mass from the mass of its progenitor (Spera et al. 2015). We are not modelling the mass-loss during neither possible episodes of Roche lobe overflows nor possible common evolution phases. Nevertheless, we set in our initial conditions a minimum orbital separation $a_{\rm in}(1 - e_{\rm in}^2) \gtrsim 10$ au to ensure that the periapsis distance of the inner binary is large enough that no common envelope phase or mass transfer occurs (Antonini et al. 2017). These processes are modelled in binary systems, but not entirely comprehended in triple systems (Di Stefano 2020; Hamers & Dosopoulou 2019).

Concerning the role of σ, we find that the larger the kick velocity the larger the total BH mass on average. This is explained in relation to our assumption of momentum-conserving kicks, where $\sigma_{\rm BH} \propto m_{\rm BH}^{-1}$. In our simulations, for $Z = 0.01$, we find that ∼50 per cent of the mergers have total mass $\gtrsim 25$ and $\gtrsim 40\,{\rm M}_\odot$ for $\sigma = 0\,{\rm km\,s^{-1}}$ and $\sigma = 100\,{\rm km\,s^{-1}}$, respectively. Increasing the mean kick velocity to $\sigma = 260\,{\rm km\,s^{-1}}$ does not change considerably the distribution of

Table 1. Total masses ($m_{\rm BH,1}+m_{\rm BH,2}$) and effective spin ($\chi_{\rm eff}$) of merging BH–BH binaries inferred by the LIGO–Virgo collaboration (LIGO Scientific Collaboration 2019a) and the IAS group (Venumadhav et al. 2019; Zackay et al. 2019).

Group	$m_{\rm BH,1}+m_{\rm BH,2}$ ($\rm M_\odot$)	$\chi_{\rm eff}$
LIGO–Virgo	$18.6^{+6.9}_{-3.9}$	$0.03^{+0.19}_{-0.07}$
LIGO–Virgo	$21.4^{+11.0}_{-5.7}$	$0.18^{+0.20}_{-0.12}$
LIGO–Virgo	$36.8^{+19.0}_{-10.3}$	$0.05^{+0.31}_{-0.20}$
LIGO–Virgo	$50.8^{+12.2}_{-10.2}$	$-0.04^{+0.17}_{-0.21}$
LIGO–Virgo	$55.8^{+8.4}_{-7.0}$	$0.07^{+0.12}_{-0.12}$
LIGO–Virgo	$58.8^{+13.4}_{-11.1}$	$0.08^{+0.17}_{-0.17}$
LIGO–Virgo	$62.1^{+11.8}_{-9.9}$	$-0.09^{+0.18}_{-0.21}$
LIGO–Virgo	$66.2^{+7.7}_{-7.5}$	$-0.01^{+0.12}_{-0.13}$
LIGO–Virgo	$68.5^{+17.9}_{-14.5}$	$0.09^{+0.22}_{-0.26}$
LIGO–Virgo	$84.2^{+25.3}_{-20.3}$	$0.37^{+0.21}_{-0.25}$
IAS	$23.2^{+8.55}_{-8.55}$	$0.25^{+0.19}_{-0.19}$
IAS	$23.3^{+6.02}_{-6.02}$	$0.27^{+0.11}_{-0.11}$
IAS	$39.3^{+9.81}_{-9.81}$	$0.05^{+0.14}_{-0.14}$
IAS	$44.1^{+9.69}_{-9.69}$	$-0.16^{+0.21}_{-0.21}$
IAS	$49.7^{+5.94}_{-5.94}$	$-0.09^{+0.09}_{-0.09}$
IAS	$52.7^{+9.34}_{-9.34}$	$0.79^{+0.11}_{-0.11}$
IAS	$55.6^{+7.06}_{-7.06}$	$-0.30^{+0.17}_{-0.17}$
IAS	$55.8^{+4.73}_{-4.73}$	$0.05^{+0.07}_{-0.07}$
IAS	$59.6^{+7.70}_{-7.70}$	$0.08^{+0.12}_{-0.12}$
IAS	$62.2^{+6.38}_{-6.38}$	$-0.05^{+0.12}_{-0.12}$
IAS	$65.1^{+4.84}_{-4.84}$	$-0.05^{+0.07}_{-0.07}$
IAS	$67.9^{+8.07}_{-8.07}$	$0.09^{+0.13}_{-0.13}$
IAS	$69.1^{+9.07}_{-9.07}$	$-0.09^{+0.20}_{-0.20}$
IAS	$74.4^{+10.5}_{-10.5}$	$0.19^{+0.19}_{-0.19}$
IAS	$76.5^{+15.0}_{-15.0}$	$0.05^{+0.26}_{-0.26}$
IAS	$78.1^{+11.2}_{-11.2}$	$-0.63^{+0.23}_{-0.23}$
IAS	$84.6^{+12.5}_{-12.5}$	$0.43^{+0.13}_{-0.13}$

total masses. Other prescriptions for the natal kicks may lead to different total mass distributions.

We report in Fig. 2 the CDF of the chirp mass, the combination of masses measured most accurately during the inspiral

$$m_{\rm chirp}=\frac{(m_{\rm BH,1}m_{\rm BH,2})^{3/5}}{(m_{\rm BH,1}+m_{\rm BH,2})^{1/5}}, \quad (5)$$

of BH–BH binaries in triples that lead to a merger, for different values of Z (top panel; $\sigma=260\,{\rm km\,s^{-1}}$) and σ (bottom panel; $Z=0.01$). As in the case of the total mass, the distribution of chirp masses is not significantly affected by the progenitor metallicity for $Z\gtrsim0.005$, ∼90 per cent of the BH–BH mergers have $m_{\rm chirp}\lesssim20\,\rm M_\odot$. We also find that ∼50 per cent of the mergers have $m_{\rm chirp}\gtrsim35\,\rm M_\odot$ and $m_{\rm chirp}\gtrsim45\,\rm M_\odot$ for $Z=0.001$ and $Z=0.0001$, respectively. Moreover, lower natal kicks predict lower chirp masses. We find that ∼50 per cent of the BH–BH mergers have $m_{\rm chirp}\gtrsim10\,\rm M_\odot$ and $m_{\rm chirp}\gtrsim18\,\rm M_\odot$ for $\sigma=0\,{\rm km\,s^{-1}}$ and $\sigma=100\,{\rm km\,s^{-1}}$, respectively. Furthermore, increasing the mean kick velocity to $\sigma=260\,{\rm km\,s^{-1}}$ does not change the distribution of chirp masses significantly. This is consistent with the results of Fragione & Loeb (2020), who studied the BH–NS mergers in triples.

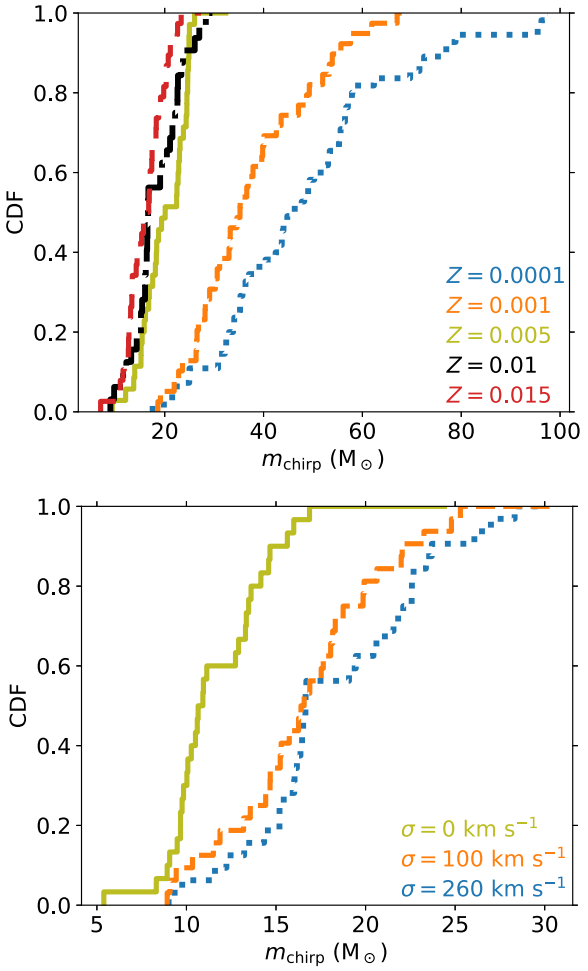

Figure 2. CDF of the chirp mass of BH–BH binaries in triples that lead to a merger, for different values of Z (top panel; $\sigma=260\,{\rm km\,s^{-1}}$) and σ (bottom panel; $Z=0.01$).

3.2 Inner and outer semimajor axis

Fig. 3 illustrates the CDF of inner (top panel) and outer (bottom panel) semimajor axis of BH–BH binaries in triples that lead to a merger for different values of the progenitor metallicity ($\sigma=260\,{\rm km\,s^{-1}}$) and mean natal kick velocities ($Z=0.01$). The progenitor metallicity does not affect the distribution of the inner and outer semimajor axes. On the other hand, the value of σ highly affects their distribution, since higher kicks unbind wider triples. We find that ∼50 per cent of the systems have $a_{\rm in}\lesssim25$, $\lesssim$60, $\lesssim$100 au for $\sigma=0$, 100, 260 $\rm km\,s^{-1}$, respectively, and ∼50 per cent of the systems have $a_{\rm out}\lesssim500$, $\lesssim$1500, $\lesssim$2500 au for $\sigma=0$, 100, 260 $\rm km\,s^{-1}$, respectively. Similar conclusions were found in Fragione et al. (2019c, d).

3.3 Eccentricity

For the BH–BH binaries that merge in our simulations, we compute a proxy for the GW frequency, i.e. the frequency corresponding to

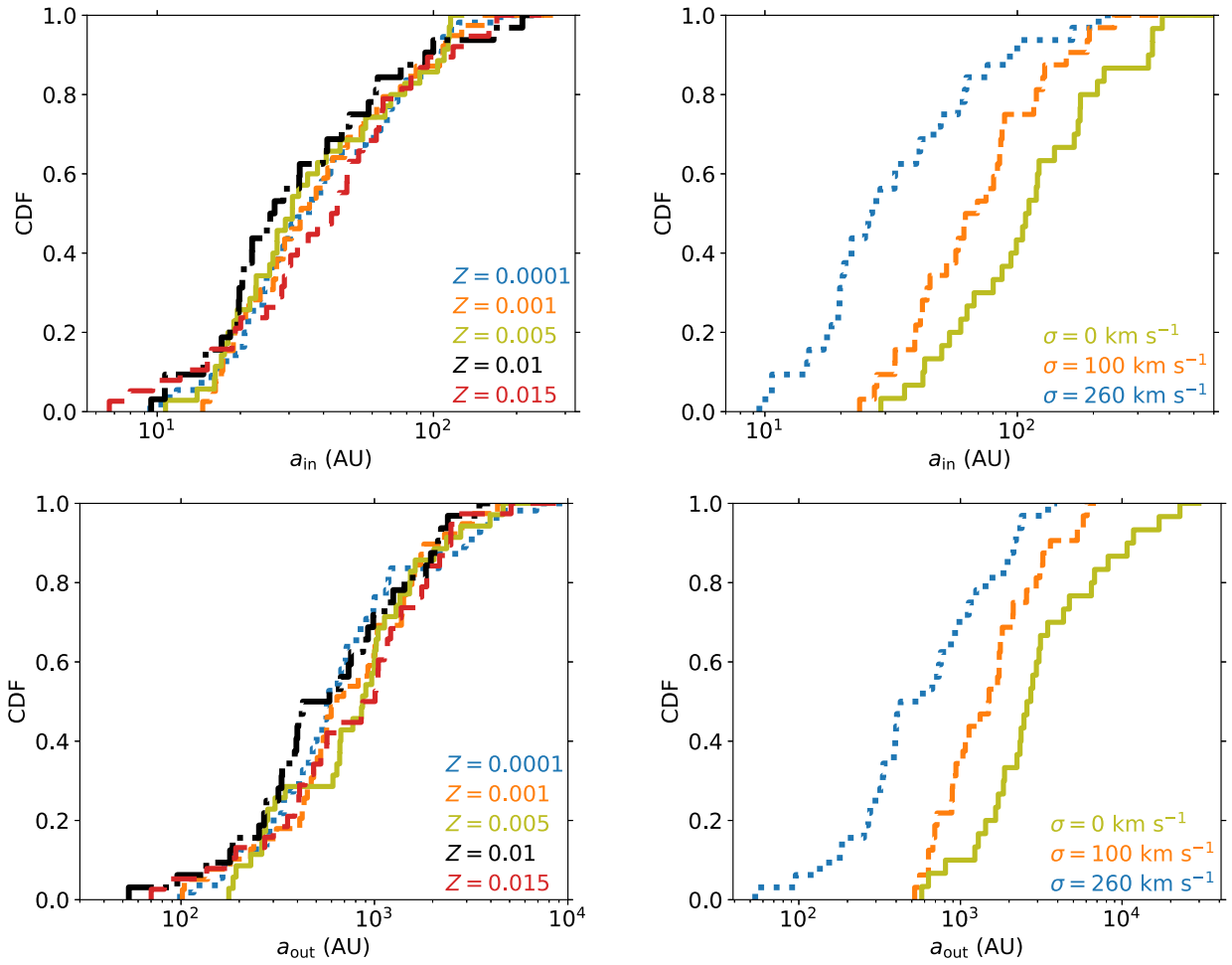

Figure 3. CDF of inner (top) and outer (bottom) semimajor axis of BH–BH binaries in triples that lead to a merger. Left-hand panel: a_{in} and a_{out} for different metallicities Z and $\sigma = 260\,\mathrm{km\,s^{-1}}$; right-hand panel: a_{in} and a_{out} for different values of σ and $Z = 0.01$.

the harmonic that gives the maximum GW emission (Wen 2003)

$$f_{\rm GW} = \frac{\sqrt{G(m_{\rm BH,1}+m_{\rm BH,2})}}{\pi}\frac{(1+e_{\rm in})^{1.1954}}{\left[a_{\rm in}\left(1-e_{\rm in}^2\right)\right]^{1.5}}. \quad (6)$$

In Fig. 4, we illustrate the probability distribution function (PDF) of eccentricities at the moment the BH binaries enter the LIGO frequency band, for Models A1, B1, and C1. We also show the minimum eccentricity $e_{10\,\rm Hz} = 0.081$ where the LIGO/VIRGO/KAGRA network may distinguish eccentric sources from circular sources (Gondán & Kocsis 2019).[4] This value is consistent with the recent LIGO/VIRGO analysis (LIGO Scientific Collaboration 2019b). A large fraction of merging BH–BH in triples retain a significant eccentricity at 10 Hz, ∼42 per cent (∼9 per cent) of the merging systems have $e_{10\,\rm Hz}$ higher than 0.023 (0.081). We note that a similar signature could be found for BH binaries that merge near supermassive and intermediate mass BHs (Fragione & Bromberg 2019; Fragione et al. 2019a; Fragione, Leigh & Perna 2019b), in the GW

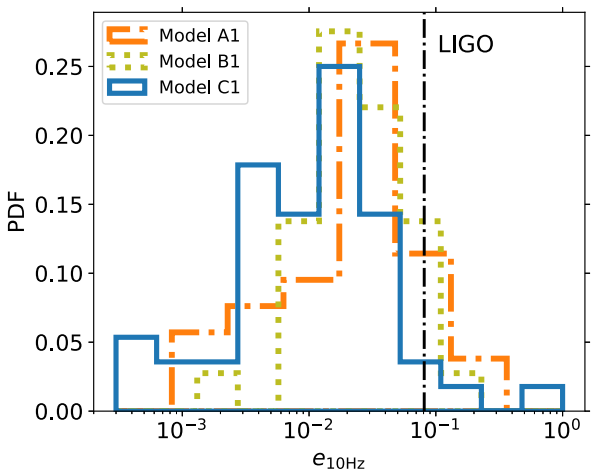

Figure 4. Distribution of eccentricities at the moment the CO binaries enter the LIGO frequency band (10 Hz) for mergers produced by triples. The vertical line shows the conservative minimum $e_{10\,\rm Hz} = 0.081$ where LIGO/VIRGO/KAGRA network may distinguish eccentric sources from circular sources (Gondán & Kocsis 2019). Note that for lower mass sources, the detection threshold at design sensitivity is $e_{10\,\rm Hz} = 0.023$, see footnote 4).

[4]Note that the detection threshold of $e_{10\rm Hz}$ varies for different binary mass. For binaries with masses of those in the LIGO observing run O1 and O2, the minimum detectable eccentricity ranges between $e_{10\,\rm Hz} = 0.023$ and 0.081 (Gondán & Kocsis 2019).

capture scenario in star clusters (Samsing 2018), and in triple (Antonini et al. 2017) and quadruple (Fragione & Kocsis 2019) systems.

3.4 Spin

In our simulations, we incorporate the spin–orbit coupling effect by introducing the spin vector $S = S\hat{S}$, where $S = (Gm_{\rm BH}^2/c)\chi$, where $0 \leq \chi \leq 1$ is the dimensionless Kerr parameter. The leading order (1.5PN) de Sitter precession of the spins $\mathbf{S_1}$ and $\mathbf{S_2}$ of the BHs in the inner binary around the inner binary angular momentum $\mathbf{J}$ is given by (Apostolatos et al. 1994)

$$\frac{{\rm d}S_1}{{\rm d}t} = \Omega_1 \times S_1 = \left[\frac{2G\mu}{c^2 r^3}\left(1+\frac{3m_2}{4m_1}\right) r \times v\right] \times S_1, \quad (7)$$

$$\frac{{\rm d}S_2}{{\rm d}t} = \Omega_2 \times S_2 = \left[\frac{2G\mu}{c^2 r^3}\left(1+\frac{3m_1}{4m_2}\right) r \times v\right] \times S_2, \quad (8)$$

where $\mu = m_1 m_2/(m_1+m_2)$ is the inner binary reduced mass, $\mathbf{r} = \mathbf{r_1} - \mathbf{r_2}$ and $\mathbf{v} = \mathbf{v_1} - \mathbf{v_2}$.[5] GW measurements are especially sensitive to the following combination of the two spins (Abbott et al. 2016; Vitale et al. 2017b)

$$\chi_{\rm eff} = \frac{m_{\rm BH,1}\chi_1 \cos\theta_1 + m_{\rm BH,2}\chi_2 \cos\theta_2}{m_{\rm BH,1}+m_{\rm BH,2}}, \quad (9)$$

where $\cos\theta_1 = (\hat{S}_1 \cdot J)/J$ and $\cos\theta_2 = (\hat{S}_2 \cdot J)/J$, where $\mathbf{J}$ is the total angular momentum of the inner BH binary, which is well approximated by the orbital angular momentum.

The magnitudes of the BH spins are expected to be set by the physics governing the stellar collapse, which depends on the progenitor star metallicity and mass-loss. However, since the specific predictions on how the progenitor properties set the remnant spin is still highly uncertain, therefore we run simulations for seven different models for the spins in order to understand how the results depend on the initial spin of the BHs. Each model differs in the initial magnitude of the Kerr spin parameter and/or the initial orientation of the spins (see Table 3)

(i) Model S1: χ_1 and χ_2 are drawn independently from an uniform distribution and angles between $0^\circ \leq \cos\theta_{1,2}^{\rm ini} \leq 20^\circ$;[6]

(ii) Model S2: χ_1 and χ_2 set by the BH mass (Belczynski et al. 2017)

$$\chi_{1,2} = \frac{p_1 - p_2}{2}\tanh\left(p_3 - \frac{M_{\rm BH1,2}}{\rm M_\odot}\right) + \frac{p_1+p_2}{2}, \quad (10)$$

where $p_1 = 0.86 \pm 0.06$, $p_2 = 0.13 \pm 0.13$, and $p_3 = 29.5 \pm 8.5$. Following Gerosa et al. (2018), spins are generated by drawing random samples uniformly in the region in between the two curves given by the upper and lower limits of the parameters. Equation (10) captures some of the key features found in Belczynski et al. (2017), that is heavier BHs tend to have smaller spins, and reflect the uncertainties of this model (see e.g. fig. 1 in Gerosa et al. 2018). The misalignment angles are drawn from $0^\circ \leq \cos\theta_{1,2}^{\rm ini} \leq 20^\circ$ uniformly;

(iii) Model T1: χ_1 and χ_2 are drawn independently from a uniform distribution and the spins are aligned with the inner angular momentum;

(iv) Model T2: χ_1 and χ_2 are drawn independently from a uniform distribution and the initial spin–orbit misalignments of the BHs are drawn from an isotropic distribution;

(v) Models U1, U2, U3: χ_1 and χ_2 are fixed at 0.2, 0.5, 0.8, respectively, and $0^\circ \leq \cos\theta_{1,2}^{\rm ini} \leq 20^\circ$ is drawn uniformly.

In Fig. 5, we show the final $\chi_{\rm eff}$ distributions of merging BH–BH binaries in triples for different values of the progenitor metallicity. In the right-hand panel of Fig. 5, we show the PDFs of the effective spins for Models U1, U2, and U3, where we fix the initial Kerr parameters of the BHs to 0.2, 0.5, 0.8, respectively. We find that mergers with high BH spins have a broadly distributed $\chi_{\rm eff}$, and mergers with low absolute spins have $\chi_{\rm eff}$ peaked around zero. The distributions do not depend significantly on the value of Z.

In the left-hand panel, we illustrate the PDFs for Models S1, S2, T1, and T2, in which the magnitude of initial spins are sampled from a broad distribution (Table 3). For these distributions, the $\chi_{\rm eff}$ distributions have a peak at $\chi_{\rm eff} \sim 0$ and broad tails, which is not significantly affected by the initial distribution of the spins. A possible exception is Model S2 for $Z = 0.0001$ and $Z = 0.001$. In these models, we sample $\chi_{\rm bh}$ from equation (10). Since low metallicities produce heavy BHs and equation (10) implies small initial spins on average, the final PDF results peak at $\chi_{\rm eff} \sim 0$ with less important tails.

In Fig. 6, we show the PDFs of $\chi_{\rm eff}$ of as function of σ. The final distributions do not depend significantly on the initial choice of the spins of the BHs in Models S1, S2, T1, T2, and presents a peak at $\sim$0 with broad tails. The only outlier is the $\chi_{\rm eff}$ distribution in the case $\sigma = 0\,{\rm km\,s^{-1}}$ for Model S2, where the distribution is flatter. In the models where we fix the Kerr parameters, the effective spin PDFs do not depend on σ and present a similar behaviour described above for different Z's. In Table 1, we report the $\chi_{\rm eff}$ inferred from observed BH–BH mergers (LIGO Scientific Collaboration 2019a; Venumadhav et al. 2019; Zackay et al. 2019). In general, some of the models are consistent with the observed distributions.

Finally, we show the distributions of the absolute misalignments θ_1 and θ_2 between $\mathbf{S_1}$ and $\mathbf{J}$ and $\mathbf{S_2}$ and $\mathbf{J}$, respectively, and $|\theta_1 - \theta_2|$ in Fig. 7. The distributions are similar to each other for the spin Models S1, S2, T1, showing that $|\theta_1 - \theta_2|$ is peaked narrowly at zero, while Model T2 shows a broader tail. Note that this is due to the fact that the initial orientation of the BH spins were drawn in a correlated way for models S1 and S2 while they are drawn independently from an isotropic distribution in Model T2. The initial correlations may be due to the interaction among progenitor stars, particularly tidal dissipation. Fig. 7 shows that the relative orientation of the BH spins do not randomize during the evolution, but they retain the information on the initial conditions. However, merging systems in triples do not show counteralignment with $|\theta_1 - \theta_2| > 90^\circ$ irrespective of the initial condition.

We do not find any significant correlation between the spin and the eccentricity in our different models. The only significant correlation is in model S2, where we use equation (10). In this case, heavier BHs tend to have smaller spins (Belczynski et al. 2017).

3.5 Merger rates

Fig. 8 shows the merger time CDFs of BH–BH binaries in triples that lead to merger for different progenitor metallicities (left; $\sigma = 260\,{\rm km\,s^{-1}}$) and different kick velocities and triple orbital parameters (right; $Z = 0.01$). In our simulations, the distribution of merger times does not depend significantly on the progenitor metallicity nor on the possible maximum separation of the triple $a_{3,\rm max}$. The only parameter on which the merger time depends significantly is the mean kick velocity, since larger values of σ

[5] We neglect the backreaction of $\mathbf{S_1}$ and $\mathbf{S_2}$ on $\mathbf{J}$ and the spin–spin precessional terms (Antonini et al. 2018; Liu et al. 2019).

[6] Here, $\cos\theta_{1,2} = \hat{S}_{1,2} \cdot \hat{L}$ describes the spin misalignment angle relative to the orbital angular momentum vector.

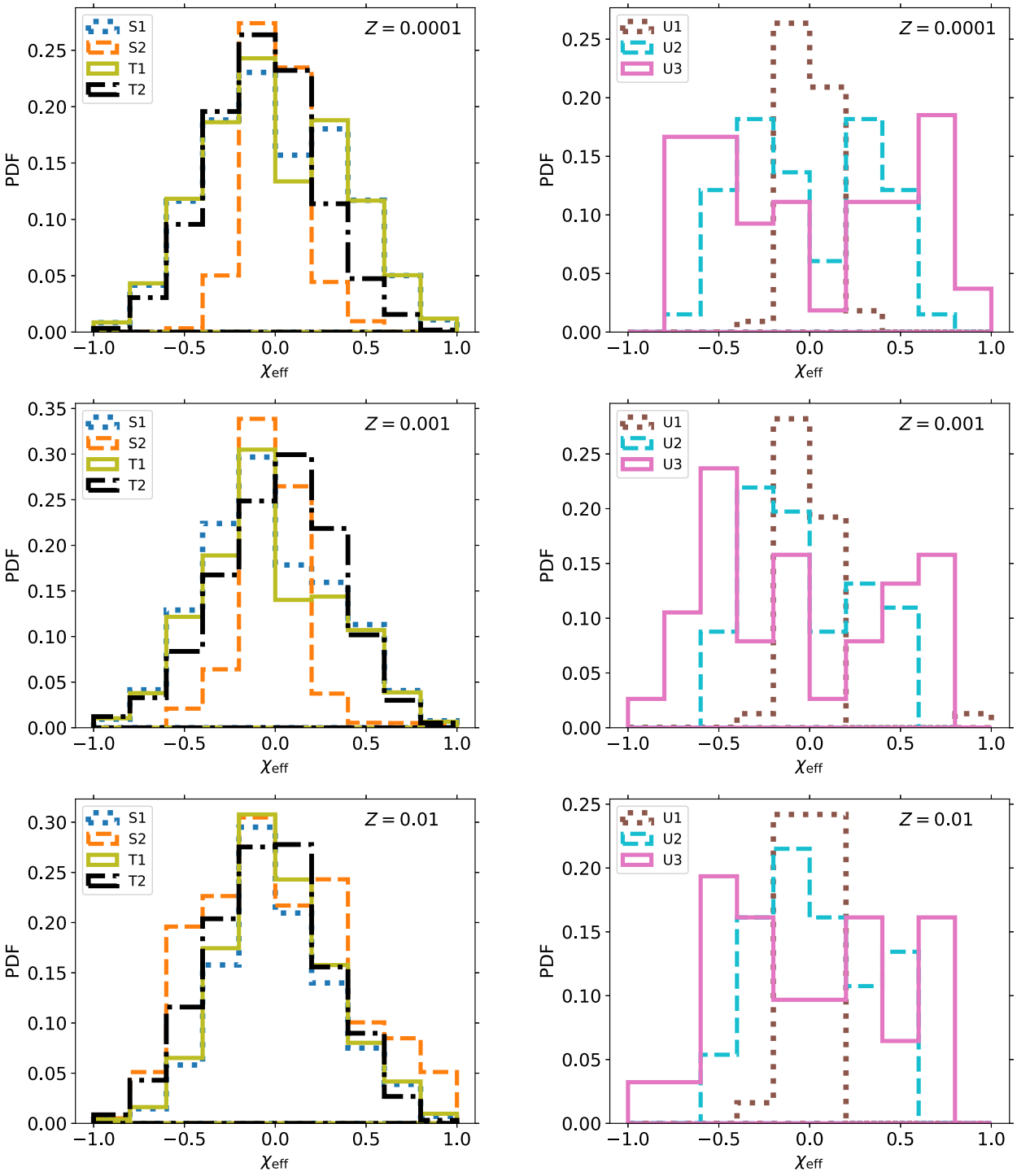

Figure 5. Effective spin distributions of BH–BH binaries in triples that lead to merger for different values of Z (top: Model B1; centre: Model A1; bottom: Model B4) and all the spin models under consideration (see Table 3).

unbind more wider triples. Therefore, triples surviving the SNe are wider for lower σ on average and merge on a longer time-scale since their LK time-scale is longer.

In order to compute the merger rate of BH–BH binaries in triples, we follow the method outlined in Silsbee & Tremaine (2017) and Fragione et al. (2019c). We assume that the local star formation rate is $0.025\,\mathrm{M}_\odot\,\mathrm{Mpc}^{-3}\,\mathrm{yr}^{-1}$ (Bothwell et al. 2011), thus the number of stars formed per unit mass, volume, and time is given by

$$\dot{n}(m) = \frac{\eta_{\rm SFR}\, f(m)}{\langle m \rangle} = 5.2 \times 10^6 \left(\frac{m}{\mathrm{M}_\odot}\right)^{-2.3} \mathrm{M}_\odot^{-1}\,\mathrm{Gpc}^{-3}\mathrm{yr}^{-1}, \quad (11)$$

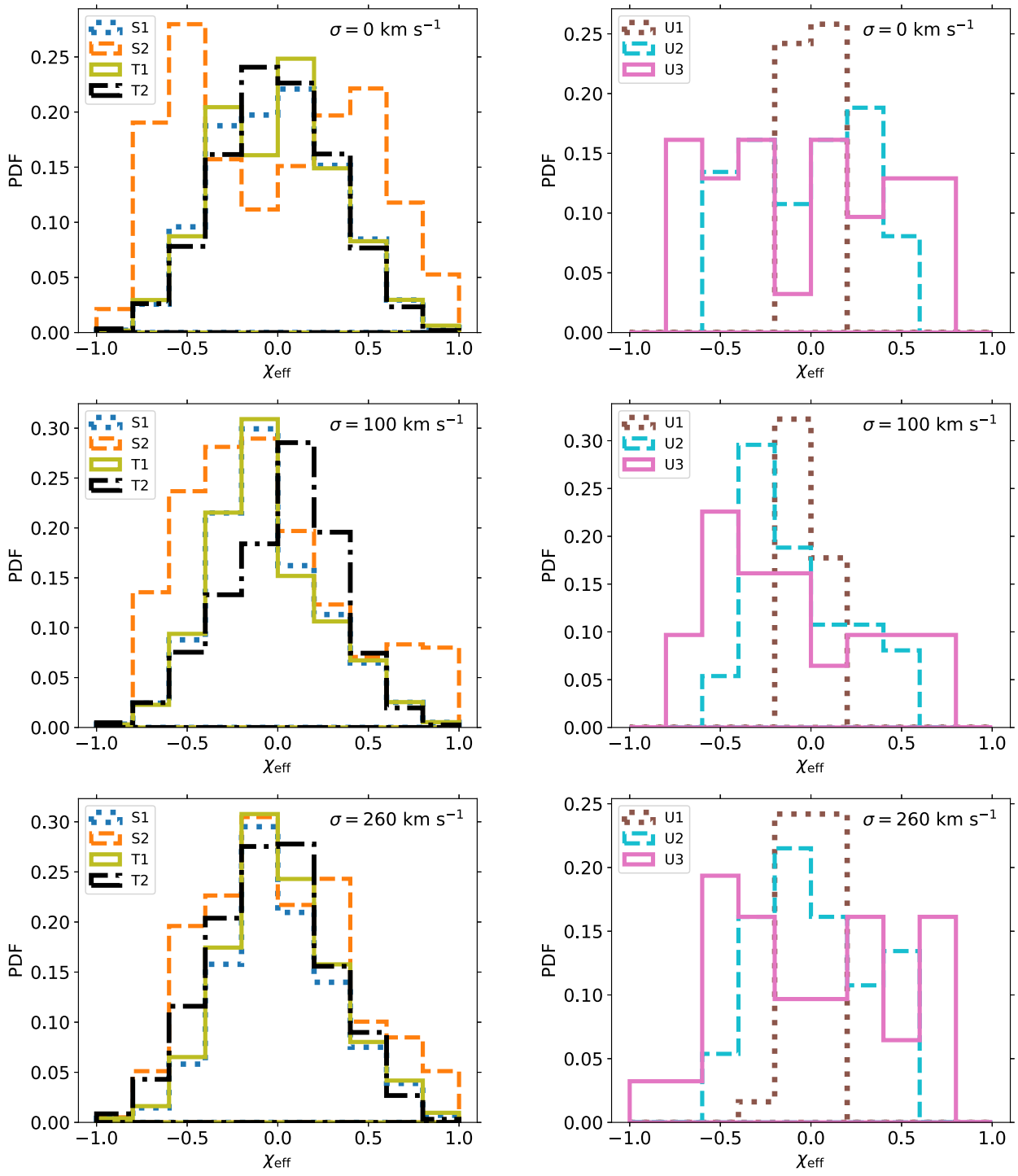

Figure 6. Effective spin distributions of BH–BH binaries in triples that lead to merger for different values of σ (top: Model A3; centre: Model A2; bottom: Model A1) and all the spin models under consideration (see Table 3).

where $\langle m \rangle = 0.38\,\mathrm{M}_\odot$ is the average stellar mass for a Kroupa mass function. Assuming a constant star formation rate,[7] the BH–BH merger rate in triple systems is then

$$\mathcal{R}_{\mathrm{BH-BH}} = (1-\zeta) f_3 f_{\mathrm{stable}} f_{\mathrm{merge}} \int_{20\,\mathrm{M}_\odot}^{150\,\mathrm{M}_\odot} \dot{n}(m_1)\mathrm{d}m_1$$

$$= 7.4 \times 10^4 \eta (1-\zeta) f_3 f_{\mathrm{stable}} f_{\mathrm{BH-BH}}\ \mathrm{Gpc}^{-3}\ \mathrm{yr}^{-1}\,, \quad (12)$$

where $f_3 = 0.25$ is the fraction of stars in triples, f_{stable} is the fraction of systems that remain stable after the SN events take place, f_{merge}

[7]The star formation rate depends on the cosmic time. Rodriguez & Antonini (2018) adopted a redshift-dependent star formation rate from Madau & Dickinson (2014) and found a similar range for the overall merger rate of triple BHs.

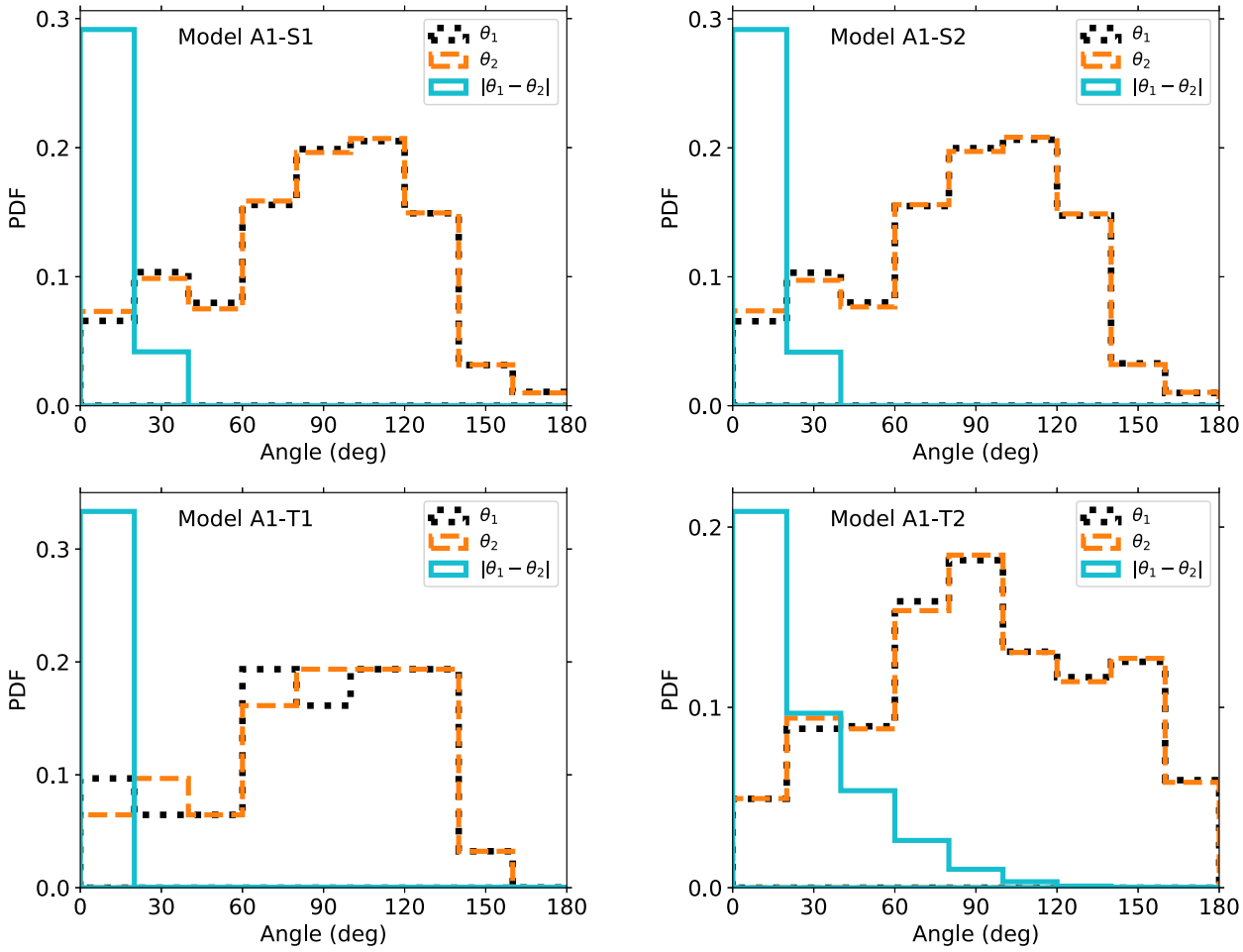

Figure 7. Distributions of the absolute misalignment θ_1 between $\mathbf{S_1}$ and $\mathbf{J}$, θ_2 between $\mathbf{S_2}$ and $\mathbf{J}$, and the relative misalignment between $\mathbf{S_1}$ and $\mathbf{S_2}$ for Model A1 and the first four spin models of Table 3.

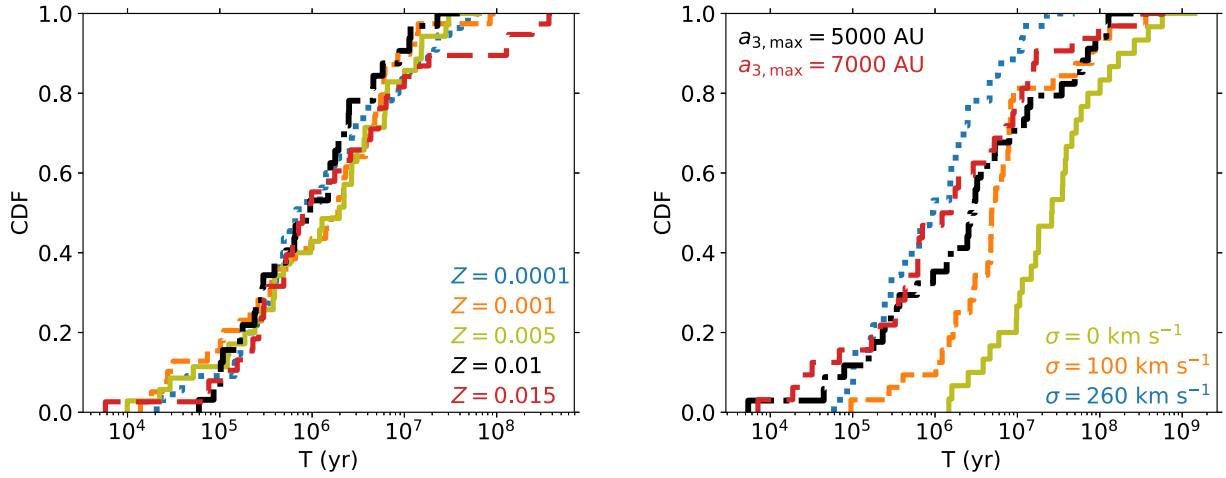

Figure 8. Merger time distribution of BH–BH binaries in triples that lead to merger (see Table 2). Left-hand panel: different progenitors metallicities and $\sigma = 260\,\mathrm{km\,s^{-1}}$; right-hand panel: different kick velocities and triple orbital parameters and $Z = 0.01$.

Table 2. Models parameters: name, dispersion of BH kick velocity distribution ($\sigma_{\rm BH}$), progenitor metallicity (Z), maximum outer semimajor axis of the triple ($a_{3,\rm max}$), fraction of stable triple systems after SNe ($f_{\rm stable}$), fraction of stable systems that merge from the N-body simulations ($f_{\rm merge}$).

Name	σ (km s^{-1})	Z	$a_{3,\rm max}$ (au)	$f_{\rm stable}$	$f_{\rm merge}$
A1	260	0.01	2000	7.8×10^{-5}	0.06
A2	100	0.01	2000	1.5×10^{-3}	0.06
A3	0	0.01	2000	3.1×10^{-2}	0.08
B1	260	0.0001	2000	1.3×10^{-1}	0.06
B2	260	0.001	2000	6.2×10^{-2}	0.06
B3	260	0.005	2000	1.4×10^{-3}	0.05
B4	260	0.015	2000	1.5×10^{-5}	0.06
C1	260	0.01	5000	5.8×10^{-5}	0.06
C2	260	0.01	7000	4.2×10^{-5}	0.05

Table 3. Spin models: name, Kerr parameter of the BH (χ), initial direction of the spins.

Name	χ	Initial direction
S1	Uniform	$0^\circ \leq \cos\theta^{\rm ini}_{1,2} \leq 20^\circ$
S2	Equation (10)	$0^\circ \leq \cos\theta^{\rm ini}_{1,2} \leq 20^\circ$
T1	Uniform	Aligned with **J**
T2	Uniform	$\cos\theta^{\rm ini}_{1,2}$ uniform
U1	0.2	$0^\circ \leq \cos\theta^{\rm ini}_{1,2} \leq 20^\circ$
U2	0.5	$0^\circ \leq \cos\theta^{\rm ini}_{1,2} \leq 20^\circ$
U3	0.8	$0^\circ \leq \cos\theta^{\rm ini}_{1,2} \leq 20^\circ$

is the fraction of systems that merge (see Table 2), and η is the conditional probability that the secondary is also a progenitor of a BH given that the primary is a BH progenitor

$$\eta = \frac{\int_{20\,{\rm M}_\odot}^{150\,{\rm M}_\odot} {\rm d}m_1\, f_{\rm IMF}(m_1) \int_{20\,{\rm M}_\odot/m_1}^{1} {\rm d}q_{12}\, f_q(q_{12})}{\int_{20\,{\rm M}_\odot}^{150\,{\rm M}_\odot} {\rm d}m_1\, f_{\rm IMF}(m_1)}, \quad (13)$$

where $f_q(q_{12})$ is the mass ratio distribution of the inner binary, which we assume to be constant. For a Kroupa (2001) initial mass function $f_{\rm IMF}$ we get $\eta = 0.38$. In equation (12), $f_{\rm merge} \sim 0.06$ for all the models, we find that the fraction of stable systems depends both on the mean natal kick and on Z, because lower progenitor metallicities lead to more massive BHs, which are on average imparted lower kicks at birth as a result of our assumption of momentum-conserving kicks (see Table 2). A factor of uncertainty is the possible KL dynamics during the evolution of the stellar triples before they form a BH–BH system in the inner binary, which we have not modelled here. Some fraction of the parameter space can be removed by the earlier evolution of the system (Shappee & Thompson 2013). To estimate this uncertainty, we assume very conservatively that any stellar triple whose initial KL time-scale is less than the lifetime of the primary star (∼7 Myr; Iben 1991; Hurley, Pols & Tout 2000; Maeder 2009) in the inner binary will merge, and, as a consequence, will not form a triple system with an inner BH–BH binary (Rodriguez & Antonini 2018). We find that the fraction of these triples is $\zeta \sim 0.83$ on average, except for Model A2 where we find $\zeta \sim 0.55$. Using the minimum and maximum values of $f_{\rm stable}$ in Table 2 and plugging numbers into equation (12)

$$\Gamma_{\rm BH-BH} = 0.008 - 9\ {\rm Gpc}^{-3}\ {\rm yr}^{-1}. \quad (14)$$

This is consistent with the merger rates in triples derived by Antonini et al. (2017) and Silsbee & Tremaine (2017). The higher merger rates correspond to low natal kicks and low progenitor metallicities. For a log-uniform distribution of mass ratios, we estimate a rate ∼2 times larger.

4 DISCUSSION AND CONCLUSIONS

Many astrophysical scenarios have been proposed to explain the BH and NS mergers observed via GW emission by the LIGO–Virgo collaboration. A promising way to disentangle the contributions from different channels is to statistically compare the distributions of masses, spins, eccentricity, and redshift of the merging binaries as discussed in Section 1. In this paper, we have studied the dynamical evolution of BH triples in isolation by means of high-precision N-body simulations, including post-Newtonian terms up to order 2.5PN. We started from the main-sequence progenitors of the BHs and modelled the SNe that lead to the formation of the BH triple. We adopted different prescriptions for the SN natal kicks, and considered different progenitor metallicities and orbital parameters. We have shown that the typical eccentricity of BH–BH binaries merging in triple systems when reaching the 10 Hz is 0.01–0.1 and that the merger rate is in the range 0.02–24 Gpc^{-3} yr^{-1}, depending on the natal kick prescriptions and progenitor metallicity, consistent with the rates inferred by Antonini et al. (2017) and Silsbee & Tremaine (2017). Higher rates correspond to low natal kicks and low metallicities. We find that the fraction of mergers with a detectable non-zero eccentricity for the LIGO–VIRGO–KAGRA network at design sensitivity is in the range ∼9–42 per cent.

We confirm the findings of Liu et al. (2019) that the BH spin exhibits a wide range of evolutionary paths, and different distributions of final spin–orbit misalignments can be produced depending on the system parameters. The effective spin parameter $\chi_{\rm eff}$ is broadly distributed if the merging BHs are highly spinning. Nevertheless, $\chi_{\rm eff}$ is peaked at zero for all triple population models that we have investigated, due to the fact that many merging systems have low intrinsic BH spins in these models, consistent with Antonini et al. (2018) and Rodriguez & Antonini (2018). We have also discussed that the triple scenario we studied in this paper could reproduce the distribution of effective spins inferred from LIGO–Virgo mergers and the IAS group (LIGO Scientific Collaboration 2019a; Venumadhav et al. 2019; Zackay et al. 2019).

We note that when we check that the triple systems remain stable after each SN event, systems that are deemed unstable by the Mardling & Aarseth (2001) criterion could still merge, thus possibly enhancing our inferred merger rates. In our calculations, we assumed that the SN events take place instantaneously and do not simulate the systems during the main-sequence lifetime of the progenitors. Nevertheless, we have used fits to single stellar evolutionary tracks to determine the final BH mass (Spera et al. 2015). However, the details of the specific evolutionary paths, which depend on stellar winds, metallicity, and rotation, of the stellar progenitors could reduce the parameter space (Shappee & Thompson 2013). The situation becomes more complicated if mass-loss during possible episodes of Roche lobe overflows and common evolution phases in the triple are considered (Di Stefano 2020; Hamers & Dosopoulou 2019). We do not model these possible effects and leave the detailed study to future investigations.

Ongoing and future observations promise to observe hundreds of merging BHs, thus providing a sufficiently high number to constrain the different formation scenarios. The GW observation of a merging BH–BH binary that enters the LIGO band with a non-negligible eccentricity and with a nearly zero effective spin would be consistent with triple scenario.

While our results show that the mass-weighted sum of the spin vectors projected on the orbital angular momentum vector, $\chi_{\rm eff}$, is approximately symmetrically distributed around $\sim$0 in the triple channel, we find that the angle between the individual spins is strictly less than $\sim$90° (Fig. 7). While this parameter is poorly constrained in the O1 and O2 observing runs, it is potentially measurable through the effects of spin precession in future longer duration detections at lower GW frequencies (see also Khan et al. 2019; Fairhurst et al. 2019). The misalignment angle between the two spins represents a powerful constraint to test the triple channel of BH mergers.

ACKNOWLEDGEMENTS

GF thanks Seppo Mikkola for helpful discussions on the use of the code ARCHAIN, and Barak Zackay for providing data on the effective spins of binary BH mergers. We thank Fabio Antonini for useful discussions. GF acknowledges support from a CIERA postdoctoral fellowship at Northwestern University. This work received funding from the European Research Council (ERC) under the European Union's Horizon 2020 Programme for Research and Innovation ERC-2014-STG under grant agreement No. 638435 (GalNUC) and from the Hungarian National Research, Development, and Innovation Office under grant NKFIH KH-125675 (to BK). This research was supported in part by the National Science Foundation under Grant No. NSF PHY-1748958.

REFERENCES

Abbott B. P. et al., 2016, Phys. Rev. Lett., 116, 241102
Antognini J. M. O., 2015, MNRAS, 452, 3610
Antonini F., Perets H. B., 2012, ApJ, 757, 27
Antonini F., Chatterjee S., Rodriguez C. L., Morscher M., Pattabiraman B., Kalogera V., Rasio F. A., 2016, ApJ, 816, 65
Antonini F., Toonen S., Hamers A. S., 2017, ApJ, 841, 77
Antonini F., Rodriguez C. L., Petrovich C., Fischer C. L., 2018, MNRAS, 480, L58
Apostolatos T. A., Cutler C., Sussman G. J., Thorne K. S., 1994, Phys. Rev. D, 49, 6274
Arca Sedda M., Benacquista M., 2019, MNRAS, 482, 2991
Arca-Sedda M., Li G., Kocsis B., 2018, preprint (arXiv:1805.06458)
Arzoumanian Z., Chernoff D. F., Cordes J. M., 2002, ApJ, 568, 289
Askar A., Szkudlarek M., Gondek-Rosińska D., Giersz M., Bulik T., 2017, MNRAS, 464, L36
Banerjee S., 2018, MNRAS, 473, 909
Bartos I., Kocsis B., Haiman Z., Márka S., 2017, ApJ, 835, 165
Belczynski K., Holz D. E., Bulik T., O'Shaughnessy R., 2016, Nature, 534, 512
Belczynski K. et al., 2017, preprint (arXiv:1706.07053)
Blaauw A., 1961, Bull. Astron. Inst. Neth., 15, 265
Bothwell M. S. et al., 2011, MNRAS, 415, 1815
Breivik K., Rodriguez C. L., Larson S. L., Kalogera V., Rasio F. A., 2016, ApJ, 830, L18
Cholis I., Kovetz E. D., Ali-Haïmoud Y., Bird S., Kamionkowski M., Muñoz J. B., Raccanelli A., 2016, Phys. Rev. D, 94, 084013
D'Orazio D. J., Samsing J., 2018, MNRAS, 481, 4775
Di Stefano R., 2020, MNRAS, 491, 495
Duchêne G., Kraus A., 2013, ARA&A, 51, 269
Fairhurst S., Green R., Hannam M., Hoy C., 2019, preprint (arXiv:1908.00555)
Farr B., Holz D. E., Farr W. M., 2018, ApJ, 854, L9
Fishbach M., Holz D. E., Farr B., 2017, ApJ, 840, L24
Fragione G., Bromberg O., 2019, MNRAS, 488, 4370
Fragione G., Kocsis B., 2018, Phys. Rev. Lett., 121, 161103
Fragione G., Kocsis B., 2019, MNRAS, 486, 4781
Fragione G., Loeb A., 2019, MNRAS, 486, 4443
Fragione G., Loeb A., 2020, MNRAS, 490, 4991
Fragione G., Grishin E., Leigh N. W. C., Perets H. B., Perna R., 2019a, MNRAS, 488, 47
Fragione G., Leigh N. W. C., Perna R., 2019b, MNRAS, 488, 2825
Fragione G., Leigh N. W. C., Perna R., Kocsis B., 2019c, MNRAS, 489, 727
Fragione G., Metzger B. D., Perna R., Leigh N. W. C., Kocsis B., 2019d, preprint (arXiv:1908.00987)
Fryer C. L., Kalogera V., 2001, ApJ, 554, 548
Gerosa D., Berti E., O'Shaughnessy R., Belczynski K., Kesden M., Wysocki D., Gladysz W., 2018, Phys. Rev. D, 98, 084036
Gondán L., Kocsis B., 2019, ApJ, 871, 178
Gondán L., Kocsis B., Raffai P., Frei Z., 2018, ApJ, 860, 5
Grishin E., Perets H. B., Fragione G., 2018, MNRAS, 481, 4907
Hamers A. S., Dosopoulou F., 2019, ApJ, 872, 119
Hamilton C., Rafikov R. R., 2019, ApJ, 881, L13
Hobbs G., Lorimer D. R., Lyne A. G., Kramer M., 2005, MNRAS, 360, 974
Hurley J. R., Pols O. R., Tout C. A., 2000, MNRAS, 315, 543
Iben I. Jr, 1991, ApJS, 76, 55
Inayoshi K., Tamanini N., Caprini C., Haiman Z., 2017, Phys. Rev. D, 96, 063014
Khan S., Chatziioannou K., Hannam M., Ohme F., 2019, Phys. Rev. D, 100, 024059
Kobulnicky H. A. et al., 2014, ApJS, 213, 34
Kocsis B., Suyama T., Tanaka T., Yokoyama S., 2018, ApJ, 854, 41
Kremer K., Chatterjee S., Breivik K., Rodriguez C. L., Larson S. L., Rasio F. A., 2018, Phys. Rev. Lett., 120, 191103
Kroupa P., 2001, MNRAS, 322, 231
Kruckow M. U., Tauris T. M., Langer N., Kramer M., Izzard R. G., 2018, MNRAS, 481, 1908
LIGO Scientific Collaboration, 2019a, Phys. Rev. X, 9, 031040
LIGO Scientific Collaboration, 2019b, preprint (arXiv:1907.09384)
Liu B., Lai D., 2017, ApJ, 846, L11
Liu B., Lai D., 2018, ApJ, 863, 68
Liu B., Lai D., 2019, MNRAS, 483, 4060
Liu B., Lai D., Wang Y.-H., 2019, ApJ, 881, 41
Lopez M. Jr, Batta A., Ramirez-Ruiz E., Martinez I., Samsing J., 2019, ApJ, 877, 56
Madau P., Dickinson M., 2014, ARA&A, 52, 415
Maeder A., 2009, Physics, Formation and Evolution of Rotating Stars. Berlin, Springer
Mandel I., Farr W. M., Colonna A., Stevenson S., Tiňo P., Veitch J., 2017, MNRAS, 465, 3254
Mardling R. A., Aarseth S. J., 2001, MNRAS, 321, 398
Meiron Y., Kocsis B., Loeb A., 2017, ApJ, 834, 200
Mikkola S., Merritt D., 2006, MNRAS, 372, 219
Mikkola S., Merritt D., 2008, AJ, 135, 2398
Naoz S., 2016, ARA&A, 54, 441
Ng K. K. Y., Vitale S., Zimmerman A., Chatziioannou K., Gerosa D., Haster C.-J., 2018, Phys. Rev. D, 98, 083007
Nishizawa A., Berti E., Klein A., Sesana A., 2016, Phys. Rev. D, 94, 064020
Nishizawa A., Sesana A., Berti E., Klein A., 2017, MNRAS, 465, 4375
O'Leary R. M., Rasio F. A., Fregeau J. M., Ivanova N., O'Shaughnessy R., 2006, ApJ, 637, 937
O'Leary R. M., Kocsis B., Loeb A., 2009, MNRAS, 395, 2127
O'Leary R. M., Meiron Y., Kocsis B., 2016, ApJ, 824, L12
Perna R., Wang Y.-H., Farr W. M., Leigh N., Cantiello M., 2019, ApJ, 878, L1
Pijloo J. T., Caputo D. P., Portegies Zwart S. F., 2012, MNRAS, 424, 2914
Postnov K., Kuranov A., 2017, Proc. IAU Symposium. 329, 118
Rasskazov A., Kocsis B., 2019, ApJ, 881, 20
Rodriguez C. L., Antonini F., 2018, ApJ, 863, 7
Rodriguez C. L., Zevin M., Pankow C., Kalogera V., Rasio F. A., 2016, ApJ, 832, L2
Rodriguez C. L., Amaro-Seoane P., Chatterjee S., Rasio F. A., 2018, Phys. Rev. Lett., 120, 151101
Samsing J., 2018, Phys. Rev. D, 97, 103014
Samsing J., D'Orazio D. J., 2018, MNRAS, 481, 5445

Samsing J., D'Orazio D. J., Askar A., Giersz M., 2018, preprint (arXiv: e-print)
Samsing J., D'Orazio D. J., Kremer K., Rodriguez C. L., Askar A., 2019, preprint (arXiv:1907.11231)
Sana H., 2017, in Eldridge J. J., Bray J. C., McClelland L. A. S., Xiao L., eds, Proc. IAU Symp. 329, The Lives and Death-Throes of Massive Stars. Kluwer, Dordrecht, p. 110
Sana H. et al., 2012, Science, 337, 444
Sana H. et al., 2013, A&A, 550, A107
Sana H. et al., 2014, ApJS, 215, 15
Schrøder S. L., Batta A., Ramirez-Ruiz E., 2018, ApJ, 862, L3
Shappee B. J., Thompson T. A., 2013, ApJ, 766, 64
Silsbee K., Tremaine S., 2017, ApJ, 836, 39
Spera M., Mapelli M., Bressan A., 2015, MNRAS, 451, 4086
Stevenson S., Ohme F., Fairhurst S., 2015, ApJ, 810, 58
Stevenson S., Berry C. P. L., Mandel I., 2017, MNRAS, 471, 2801
Stone N. C., Metzger B. D., Haiman Z., 2017, MNRAS, 464, 946
Tagawa H., Saitoh T. R., Kocsis B., 2018, Phys. Rev. Lett., 120, 261101
Tagawa H., Haiman Z., Kocsis B., 2019, preprint (arXiv:1912.08218)
Talbot C., Thrane E., 2017, Phys. Rev. D, 96, 023012
Toonen S., Hamers A., Portegies Zwart S., 2016, Comput. Astrophys. Cosmol., 3, 6
Venumadhav T., Zackay B., Roulet J., Dai L., Zaldarriaga M., 2019, preprint (arXiv:1904.07214)
Vitale S., Lynch R., Sturani R., Graff P., 2017a, Class. Quantum Gravity, 34, 03LT01
Vitale S., Lynch R., Raymond V., Sturani R., Veitch J., Graff P., 2017b, Phys. Rev. D, 95, 064053
Wen L., 2003, ApJ, 598, 419
Yang Y. et al., 2019a, Phys. Rev. Lett., 123, 181101
Yang Y., Bartos I., Haiman Z., Kocsis B., Márka Z., Stone N. C., Márka S., 2019b, ApJ, 876, 122
Zackay B., Venumadhav T., Dai L., Roulet J., Zaldarriaga M., 2019, Phys. Rev. D, 100, 023007
Zaldarriaga M., Kushnir D., Kollmeier J. A., 2018, MNRAS, 473, 4174
Zevin M., Pankow C., Rodriguez C. L., Sampson L., Chase E., Kalogera V., Rasio F. A., 2017, ApJ, 846, 82
Zevin M., Samsing J., Rodriguez C., Haster C.-J., Ramirez-Ruiz E., 2019, ApJ, 871, 91

This paper has been typeset from a TEX/LATEX file prepared by the author.